IJRCS

International Journal of Robotics and Control Systems
Vol. 5, No. 3, 2025, pp. 2053-2067
ISSN 2775-2658
http://pubs2.ascee.org/index.php/ijrcs

ASCEE

Chess Optimizer for Load Frequency Control of Three-Area Multi-Source Renewable Energy Based on PID Plus Second Order Derivative Controller

Chatmongkol Areeyat [a,1], Sitthisak Audomsi [a,2], Jagraphon Obma [b,3], Xiaoqing Yang [c,4], Worawat Sa-Ngiamvibool [a,d,5,*]

[a] Faculty of Engineering, Mahasarakham University, Maha Sarakham, 44150, Thailand
[b] Department of Computer Engineering, Rajamangala University of Technology ISAN, Khonkaen Campus, Khon Kaen, Thailand
[c] Shanxi Vocational University of Engineering Science and Technology, Shanxi, China
[d] Electrical and Computer Engineering Research Unit, Mahasarakham University, Maha Sarakham 44150, Thailand
[1] 67010353011@msu.ac.th; [2] Sitthisak.seagame@gmail.com; [3] Jagraphon.ob@rmuti.ac.th; [4] Yangxqmty0907@163.com; [5] Wor.nui@gmail.com
* Corresponding Author

ARTICLE INFO

Article history
Received July 05, 2025
Revised August 10, 2025
Accepted October 08, 2025

Keywords
Chess Optimizer;
Load Frequency Control;
PID Plus Second-Order Derivative Controller;
Three-Area Multi-Source

ABSTRACT

Renewable energy sources such as solar and wind are increasingly integrated into multi-area power systems. However, their fluctuating and unpredictable characteristics pose challenges for sustaining system stability. Therefore, automatic generation control (AGC) is essential for the continual regulation of power and frequency in the system. This article presents the use of a Proportional–Integral–Derivative plus second-order derivative (PID+DD) controller for load frequency control in a three-area multi-source power system, which includes a thermal reheat power plant with a generation rate constraint (GRC) representing the maximum permissible change rate of generation output of 5% per min , a hydroelectric power plant with a GRC of 370% per min, and a wind power plant where wind speeds vary across areas. The power generation ratio of the three areas is 1:2:4. The controller parameters were tuned using a Chess Optimizer (CO), a metaheuristic inspired by chess move complexity and planning, with specific weights assigned to each type of chess piece. Two load change scenarios were studied: a 10% step load perturbation (10% SLP) and a random load pattern (RLP). Furthermore, experimental results based on the Integral of Time-weighted Absolute Error (ITAE) indicate that the PID+DD controller tuned by the Chess Optimizer achieved the lowest steady-state error in both scenarios (10% SLP and RLP). In Case 1 (SLP), it achieved an ITAE of 25.5072, representing a 9.70% reduction compared to the PID controller and a 1.96% reduction compared to the PI controller. In Case 2 (RLP), it achieved an ITAE of 88.0654, representing a 1.14% reduction compared to the PID controller and a 2.03% reduction compared to the PI controller. These improvements contribute to enhanced oscillation damping, reduced overshoot and undershoot, and improved frequency stability, demonstrating the practical applicability of the proposed approach in future smart grids with high renewable energy penetration.

1. Introduction

The global energy sector is transitioning to renewable energy systems to ensure long-term sustainability. The addition of renewable energy sources such as solar and wind, into multi-area power networks is growing as an important trend. The inconsistent and fluctuating character of this renewable energy makes it difficult to maintain system stability when it is integrated into primary power producing systems. Therefore, Automatic Generation Control (AGC) [1], [2] and [3] developed as an essential part for the continual regulation of energy and frequency inside the system [4], [5] and [6].

The PID controller, although prevalent in automated control systems [7] because of its design simplicity and satisfactory performance [8], [9] and [10] in many cases, has significant limits when used in complex or highly unpredictable systems. A primary drawback is its ability to respond to sudden disturbances or rapid load fluctuations, potentially causing overshoot, undershoot, or oscillations, making it unsuitable for modern systems that need high flexibility and adaptability [11]-[13] and [14].

A review of the literature on Load Frequency Control (LFC), including single-source [15]-[17] and [18] dual-source [19] and multiple-source [20]. For example, More Raju [21] studied AGC in a three-area thermal reheat system using I, PI, PID, and PID+DD controllers [22], tuned with the ALO algorithm. The results showed that PID+DD outperformed in terms of settling time, overshoot, and stability, even in cases of random load changes. The documents [23]-[25] and [26] study ACG systems using different controllers, including algorithms such as PSO and GWO [27]-[29] and [30]. Sitthisak Audomsi [31] studies the development of LFC system controllers using the Chess algorithm (CA), comparing it with other algorithms and finding that CA yields better results than PSO. [32], [33] and [34] studies multi-source frequency systems with renewable energy, where wind power is one of the sources.

The Chess Optimizer (CO), obtaining inspiration from the unique movement patterns of chess pieces, provides a unique balance between global exploration and local exploitation, enhancing its susceptibility to premature convergence as compared to GA, PSO, or GWO. This research utilizes CO to enhance the parameters of a PID+DD controller within nonlinear multi-area power systems. This approach improves global search capability, minimizes the risk of converging to suboptimal solutions, and enhances system stability and dynamic response in continuously changing load demands and variable renewable energy generation.

2. Methodology

2.1. System and Model Configuration

The three-area multi-source power plant in this context consists of a thermal reheat power plant, a hydraulic power plant with wind power plants, and a thermal reheat power plant with wind power plants, as shown in Fig. 2. The maximum generation capacity of each area is 1,000 MW, 2,000 MW, and 4,000 MW, respectively, or in the ratio of 1:2:4. Each type of power plant has its own production constraints: the thermal reheat power plant has a GRC of 5% per min, and the hydraulic power plant has a GRC of 370% per min. The parameters of the power system transfer function are presented in Appendix A. This study proposes the use of a PID+DD controller and compares it to conventional controllers, such PID, and PI, using the Chess Optimizer to find the parameters of these controllers. Case studies include 10% SLP and RLP, as shown in Fig. 1. The optimum values were determined by a cost function, ITAE, as defined in Equation (1) [35], [36] and [37].

$$\mathrm{ITAE} = \int_0^{t_{sim}} t \cdot (|\Delta f_i| + |\Delta P_{tie\text{-}i}|) dt \quad (1)$$

The Area Control Error (ACE) [38] is a composite signal that integrates the tie-line power exchange and the frequency deviation feedback. It functions as the principal input for managing power

system variations in interconnected multi-area networks. The mathematical formulation of ACE is presented in Equations (2) and (3).

$$\Delta P_{tie,i} = 2\pi \left[\sum_{\substack{j=1 \\ j \neq i}}^{N} T_{ij} \Delta f_i - \sum_{\substack{j=1 \\ j \neq i}}^{N} T_{ij} \Delta f_j \right] \tag{2}$$

$$ACE_i = B \cdot \Delta f_i + \Delta P_{tie,i} \tag{3}$$

where i represent the area number (i = 1, 2, ... , n)

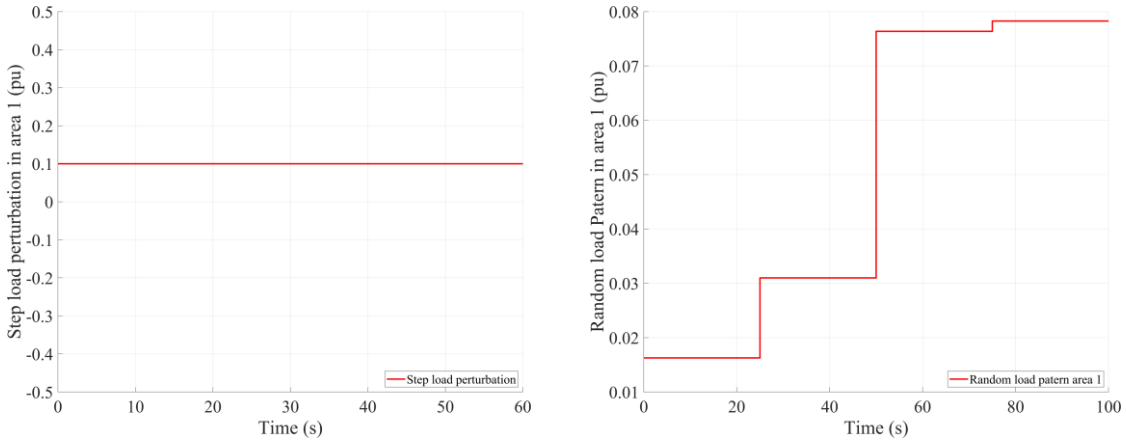

(a) (b)

Fig. 1. Load disturbance (a) Step load perturbation (SLP) (b) Random load pattern (RLP)

2.1.1. Thermal Reheat Power Plants

The modeling of a thermal reheat power plant comprises three primary components: the governor, the steam turbine, and the reheater. All of these components demonstrate nonlinear behavior and are constrained by physical limitations, including the GRC, as referenced in [39]-[43] and [44].

The transfer function of a thermal reheat power plant, shown as $G_{Thermal}(s)$, can be divided into three primary components, each depicting the dynamic behavior of an important subsystem inside the thermal unit: the speed governor, the steam turbine, and the reheater. Equation (4) defines the mathematical representation of the transfer functions connected to each of these components [45] and [46].

$$G_{thermal}(s) = \left[\frac{1}{1 + sT_G} \right] \left[\frac{1}{1 + sT_T} \right] \left[\frac{1 + sK_R T_R}{1 + sT_R} \right] \tag{4}$$

Where T_G is the time constant that defines the delay linked to the mechanical actuation of the governor, T_T is the time constant that indicates the delay in the conversion of thermal energy into mechanical power, T_R is the time constant of the reheater, and K_R is the reheating gain coefficient, denoting the proportion of steam reintroduced into the reheating process. The parameter values of thermal reheat power plant models are shown in Appendix A.

2.1.2. Hydropower Plants

The dynamic behavior of a hydropower plant [47]-[49] and [50], the primary components of the system can be divided into three primary components: the hydraulic governor, the drop compensation system, and the hydraulic turbine. These components directly affect the system's response to variations in electrical load. The system can be represented in Equation (5).

$$G_{Hydro}(s) = \left[\frac{1}{1 + sT_{H1}} \right] \left[\frac{1 + sT_{H2}}{1 + sT_{H3}} \right] \left[\frac{1 - sT_W}{1 + 0.5\, sT_W} \right] \tag{5}$$

Where the time constant T_{H1} dictates the extent of system inertia and response delay, T_{H2} and T_{H3} dictate the configuration of the dynamic response, enabling it to more effectively adapt to the particular characteristics of load variations. The measure T_W, known as the water starting time, denotes the duration necessary for water flow to commence turbine spinning. All specific parameter values used in this hydropower plant model are detailed in Appendix A.

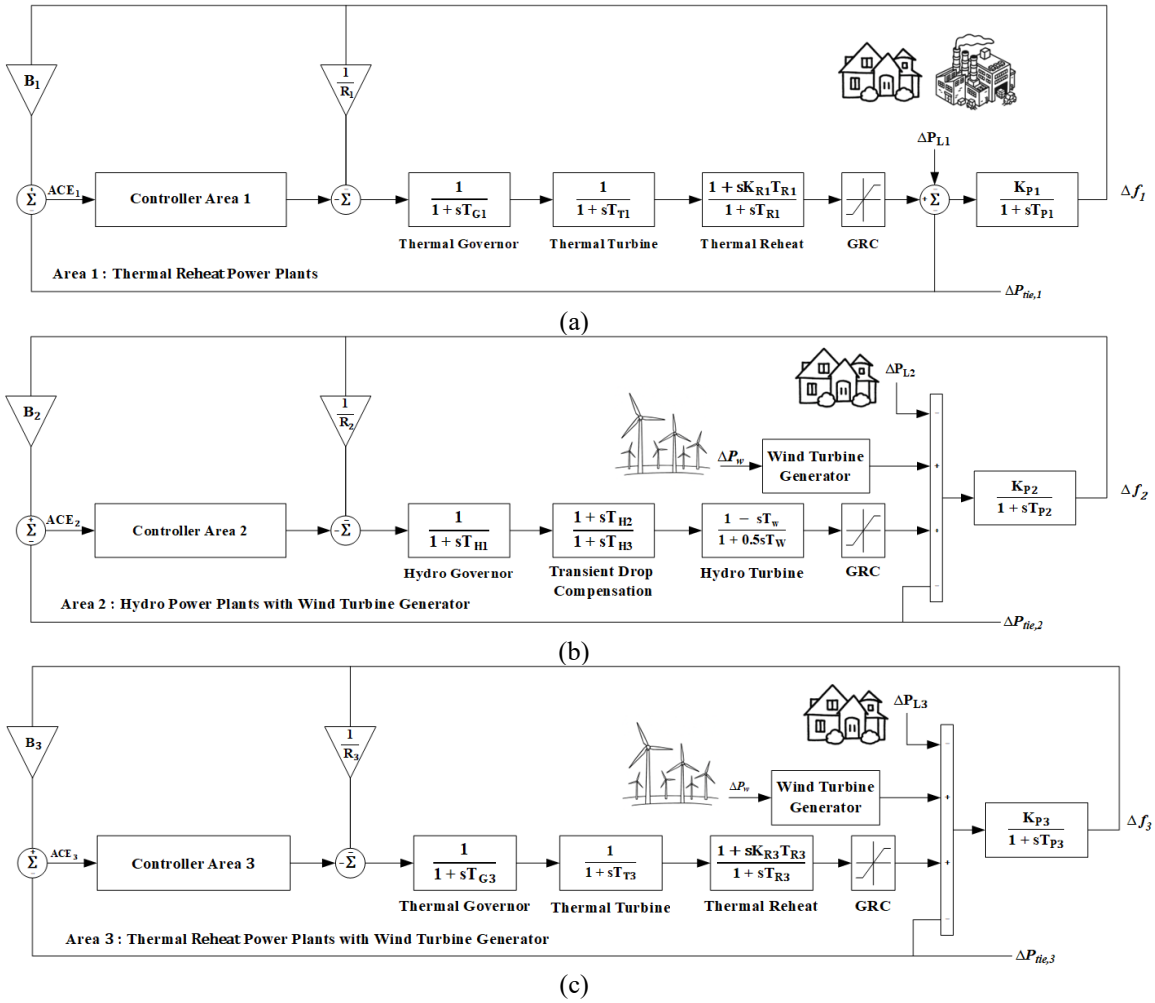

Fig. 2. Three-area multi-source renewable energy (a) Thermal power plant in area 1 (b) Hydropower plant and wind turbine generator in area 2 (c) Thermal power plant and wind turbine generator in area 3

2.1.3. Wind Power Plants

Wind power generation [46], [51], [52] and [53] is a discontinuous and nonlinear system due to the constantly changing nature of the wind. The wind speed varies unexpectedly, leading to instability and significant variability in the electrical output generated by the wind turbines. To respond to such characteristics, a wind speed model that changes over time was created using MATLAB/SIMULINK, shown in Fig. 3, that is a wind power generation source model.

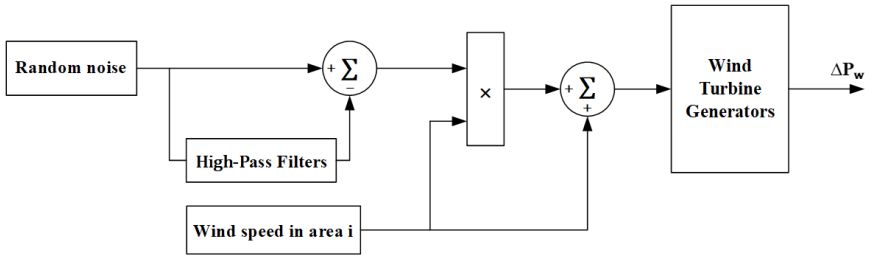

Fig. 3. Wind power generation source model

This model starts with a white noise signal block to provide a random signal that represents the inherent unpredictability of the wind. The signal is processed using a system characterized by a transfer function of $\frac{300s}{1+300s}$, functioning as a high-pass filter to reduce low-frequency signals and accentuate fast variations. The filtered random signal is then combined with a steady wind speed (like the average wind) from the Wind Speed block, and the total is sent to a multiplication block (X) to simulate variations in wind speed over time.

The electrical power production of a wind turbine is directly contingent upon the instantaneous wind speed. The extractable wind power can be determined using equation (6), Where P_W is the power that can be generated (W), ρ is the air density (kg/m^3), V_W is the wind speed at that time (m/s), A_T is the wind-facing area of the blades (m^2) and λ_T is the turbine characteristics, which means that when the wind speed variations, the pitch angle of the blades will also change accordingly, as shown in the equation (7).

$$P_W = \frac{1}{2}\rho A_T V^3 C_p(\lambda,\beta) \tag{6}$$

$$\lambda_T = \frac{\omega_T \cdot R_T}{V_W} \tag{7}$$

Variable-speed wind turbines are engineered to function by sustaining an appropriate tip speed ratio (TSR), referred to as the relative TSR (λ_i), in the context of fluctuating wind speeds, rather than permitting it to vary with changing wind conditions. This method guarantees optimal aerodynamic efficiency and power extraction. The value of λ_i can be determined using Equation (8).

$$\frac{1}{\lambda_i} = \frac{1}{\lambda_T + 0.08\beta} - \frac{0.035}{\beta^3+1} \tag{8}$$

The power coefficient (C_p) is the ratio of extracted wind power to the total available wind power. The relationship is determined by the TSR (λ) and the blade pitch angle (β). The value of $C_p(\lambda, \beta)$ may be determined using Equation (9).

$$C_P(\lambda,\beta) = C_1\left(\frac{C_2}{\lambda_i} - C_3\beta - C_4\beta^2 - C_5\right)\cdot e^{-\frac{C_6}{\lambda_i}} + C_7\lambda_T \tag{9}$$

The time-varying wind speed signal obtained from the multiplication procedure illustrates the inherently flexible and unpredictable nature of wind activity. The signal is then sent to the wind turbine generator (WTG) model, which converts the variable wind input into electrical power output. The output signal, denoted as ΔP_W, indicates the variation in electrical power generated by wind in response to variations in wind speed and shown in Fig. 4. Appendix A provides detailed system parameters and model configuration.

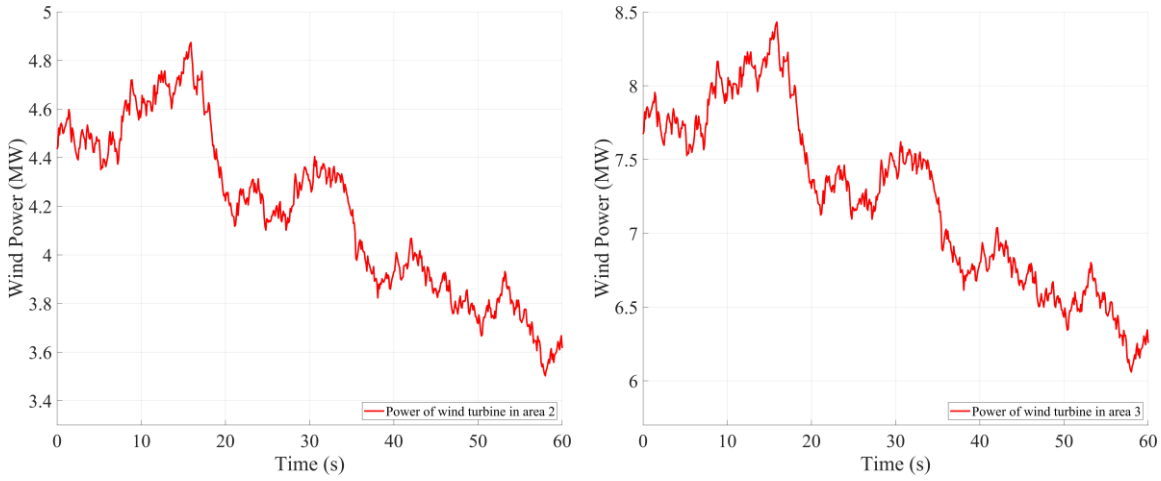

Fig. 4. Wind power (a) wind power in area 2 (b) wind power in area 3

2.2. Boundary of Parameter Search

The search boundaries for the desired parameters, Kp, Ki, Kd, and Kdd, have been defined in this experiment to control the exploration of the chess Optimizer within a range that is in tune with the system's properties. These boundaries are set within the range [0, 1]. This range is commonly adopted in metaheuristic optimization because it allows parameters to be normalized, which simplifies the tuning process, enhances search stability, and prevents values from exceeding the physical limits of the system. Furthermore, to provide an equitable comparison of each controller, the iterations and beginning population size are standardized throughout all experiments [54], [55] and [56]. This procedure attempts to mitigate any bias caused by varying iteration counts or population sizes, thereby enabling a fair and unbiased assessment of each controller's search efficiency [57].

2.3. PID Plus Second Order Derivative Controller

The PID controller [58]-[61] 20and [62] is common in control systems with automation because of its simple structure and effective performance in controlling different systems. However, in systems with high uncertainty or a sudden shift, conventional PID may not respond adequately. To reduce this constraint, a PID controller including second-order derivative terms has been developed, allowing the system to evaluate deviations with higher accuracy and quickly. This results in more accurate and stable system responses, particularly if the system has complex dynamics or high uncertainty. The design of this controller may be represented as a transfer function in accordance with Equation (10) and its structure is shown in Fig. 5.

$$R(s) = K_p + \frac{K_i}{s} + K_d s + K_{dd} s^2 \tag{10}$$

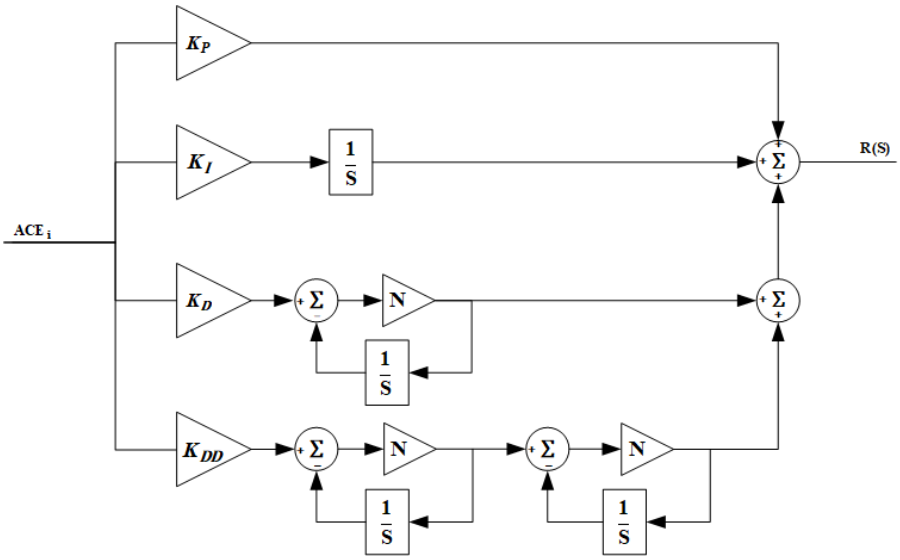

Fig. 5. Structure of PID plus second-order derivative

2.4. Chess Optimizer

The chess Optimizer is inspired by international chess, with a focus on intricacy and strategic planning. Each type of piece on the board has unique movement patterns and characteristics. Pawns serve as the vanguard, probing new areas or creating defensive positions. The rook could control a wide area in a linear trajectory. The knight can leap over pieces and formulate unforeseen plans. The bishop moves diagonally, establishing angles of assault. The queen can traverse in all directions, facilitating optimal exploration and combat efficacy. The king is the pivotal element that requires protection and epitomizes the optimal solution for the system. The unique movement characteristics of each piece facilitate the application of this approach to discover optimum values by assigning weights or significance to the motions of each piece during the exploration of novel solutions in each

search iteration. Pieces with high potential may be given opportunities to explore positions that are expected to be good. The integration of movement patterns and piece tactics, together with the configuration of movement weights, allows the algorithm to sustain balance between both exploration and extraction. The chess Optimizer is adept at addressing complex optimization challenges that need flexibility in the search process. The workflow diagram is shown in Fig. 6.

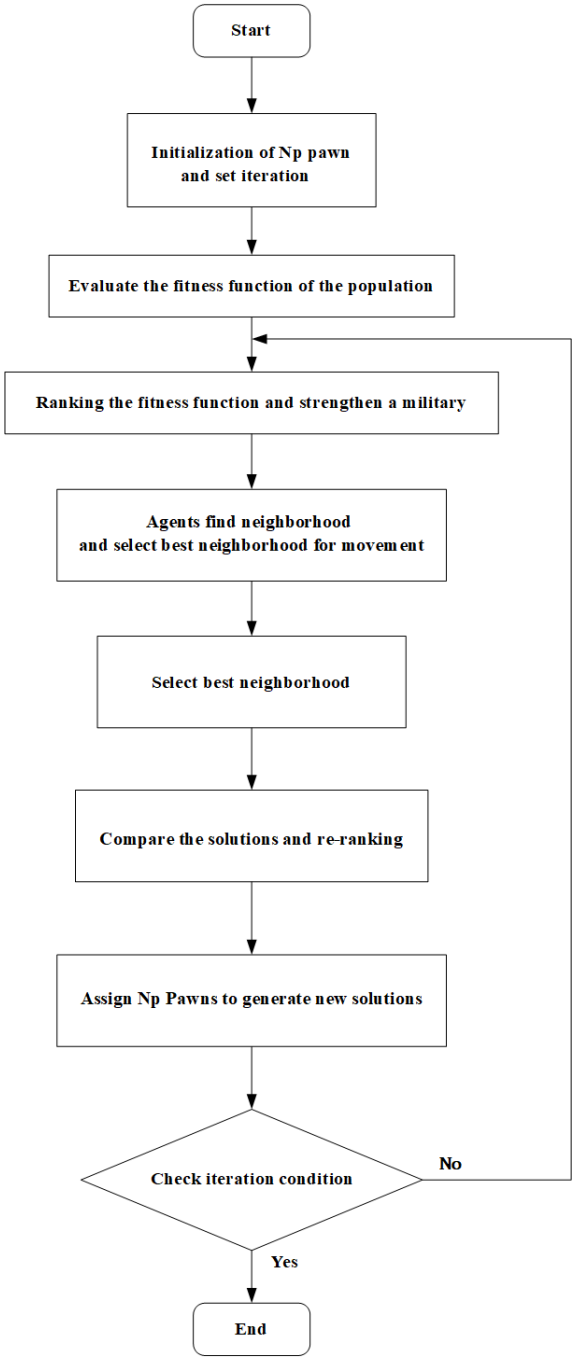

Fig. 6. Flowchart of chess optimizer

3. Results and Discussion

3.1. Study Case: Step Load Perturbations 10 % (10% SLP)

SLP simulates a sudden and fixed change in load, frequently utilized in control system testing to assess transient response and stability margins. The Chess Optimizer was used to tune the parameters

of controllers such as PI, PID, and PID+DD. In Case Study 1, the optimal values for the PI Controller were Kp1 = 0.0576, Ki1 = 0.2644, Kp2 = 0.2332, Ki2 = 0.9925, Kp3 = 0.7848, and Ki3 = 0.1733. The PID controller parameters are Kp1 = 0.0098, Ki1 = 0.4140, Kd1 = 0.1018, Kp2 = 0.2666, Ki2 = 0.7075, Kd2 = 0.3175, Kp3 = 0.9834, Ki3 = 0.1964, and Kd3 = 0.5882. The PID+DD controller parameters are Kp1 = 0.0618, Ki1 = 0.2400, Kd1 = 0.9875, Kdd1 = 0.2418, Kp2 = 0.1318, Ki2 = 0.9322, Kd2 = 0.5836, Kdd2 = 0.8511, Kp3 = 0.9880, Ki3 = 0.2285, Kd3 = 0.7692, and Kdd3 = 0.5377. The dynamic response shown in Fig. 7 (a)-(f). The result of case 1 shown in Table 1.

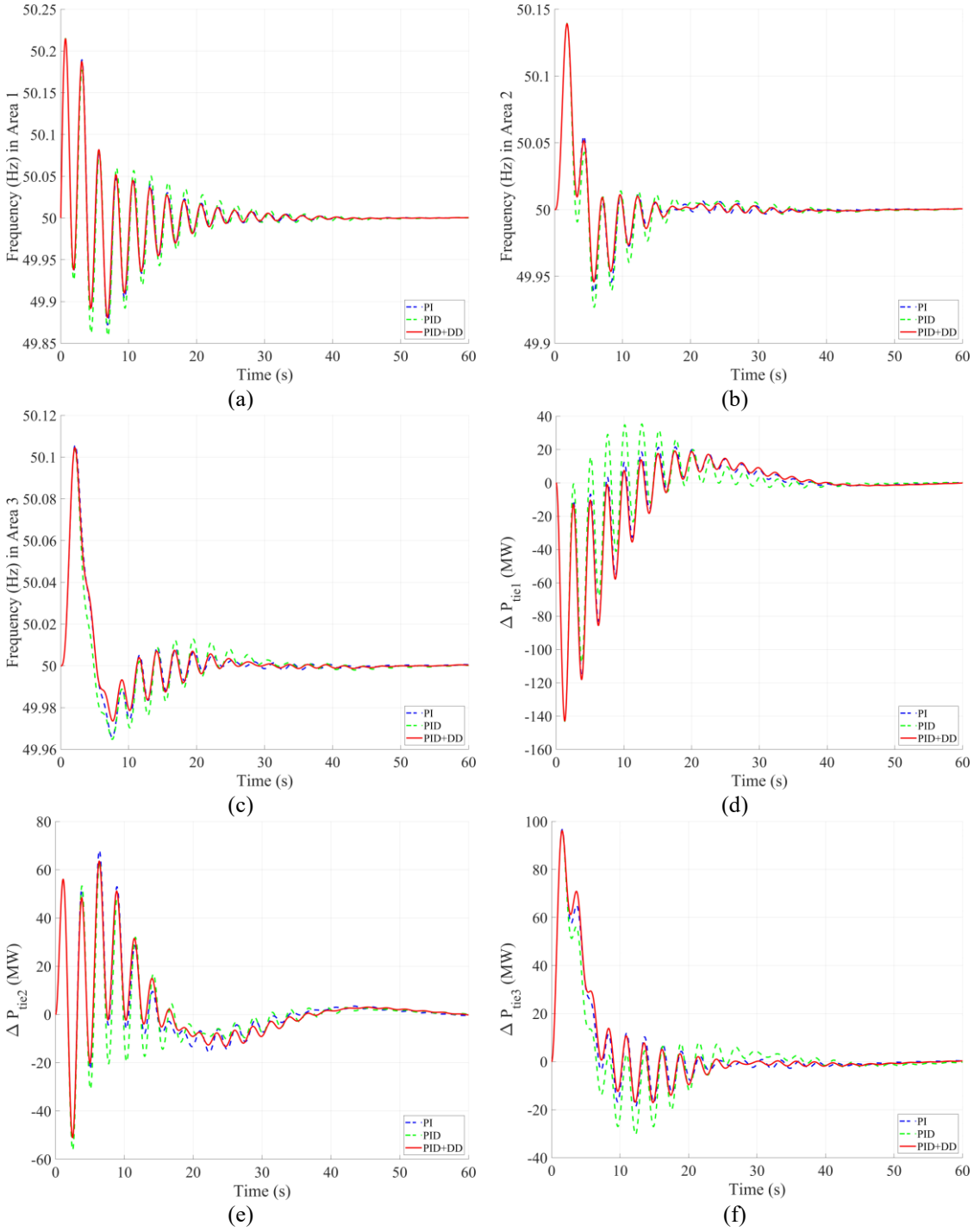

Fig. 7. Frequency and power deviations in case 1, 10% RLP (a) Frequency deviations in thermal reheat power plants area 1 (b) Frequency deviations in hydropower plants area 2 (c) Frequency deviations in thermal reheat power plants area 3 (d) Power deviations in thermal reheat power plants area 1 (e) Power deviations in hydropower plants area 2 (f) Power deviations in thermal reheat power plants area 3

Table 1. The result of case 1

		f_1 (Hz)	f_2 (Hz)	f_3 (Hz)	$P_{tie,1}$ (MW)	$P_{tie,2}$ (MW)	$P_{tie,3}$ (MW)
PID+DD	**Overshoot**	50.2145	50.1391	50.1044	19.0561	63.5009	96.1156
	Undershoot	49.8808	49.9459	49.9736	-142.8668	-51.0418	-17.0647
	Settling time	23.3397	13.8194	15.6944	27.8488	11.9309	4.6398
	ITAE	25.5072					
PID	**Overshoot**	50.2149	50.1393	50.1038	35.2563	63.4280	96.0669
	Undershoot	49.8588	49.9270	49.9648	-143.0781	-56.2325	-30.3429
	Settling time	28.5581	16.3000	22.3697	23.1468	12.0139	4.3000
	ITAE	28.2478					
PI	**Overshoot**	50.2146	50.1392	50.1057	21.5090	68.0561	96.5969
	Undershoot	49.8721	49.9381	49.9658	-143.0661	-51.5155	-18.6591
	Settling time	25.7240	13.8000	15.7587	27.8163	11.9309	4.6199
	ITAE	26.0160					

3.2. Study Case: Random Load Pattern (RLP)

RLP mimics the unpredictable changes in demand, accurately representing the operational unpredictability presented in real-world situations caused by evolving consumer consumption patterns and the instability of renewable energy sources. The simulation of these two scenarios facilitates the assessment of the controller's efficacy in both predicted and unanticipated disturbances, guaranteeing that the findings cover a broad spectrum of operating situations while preserving simulation simplicity.

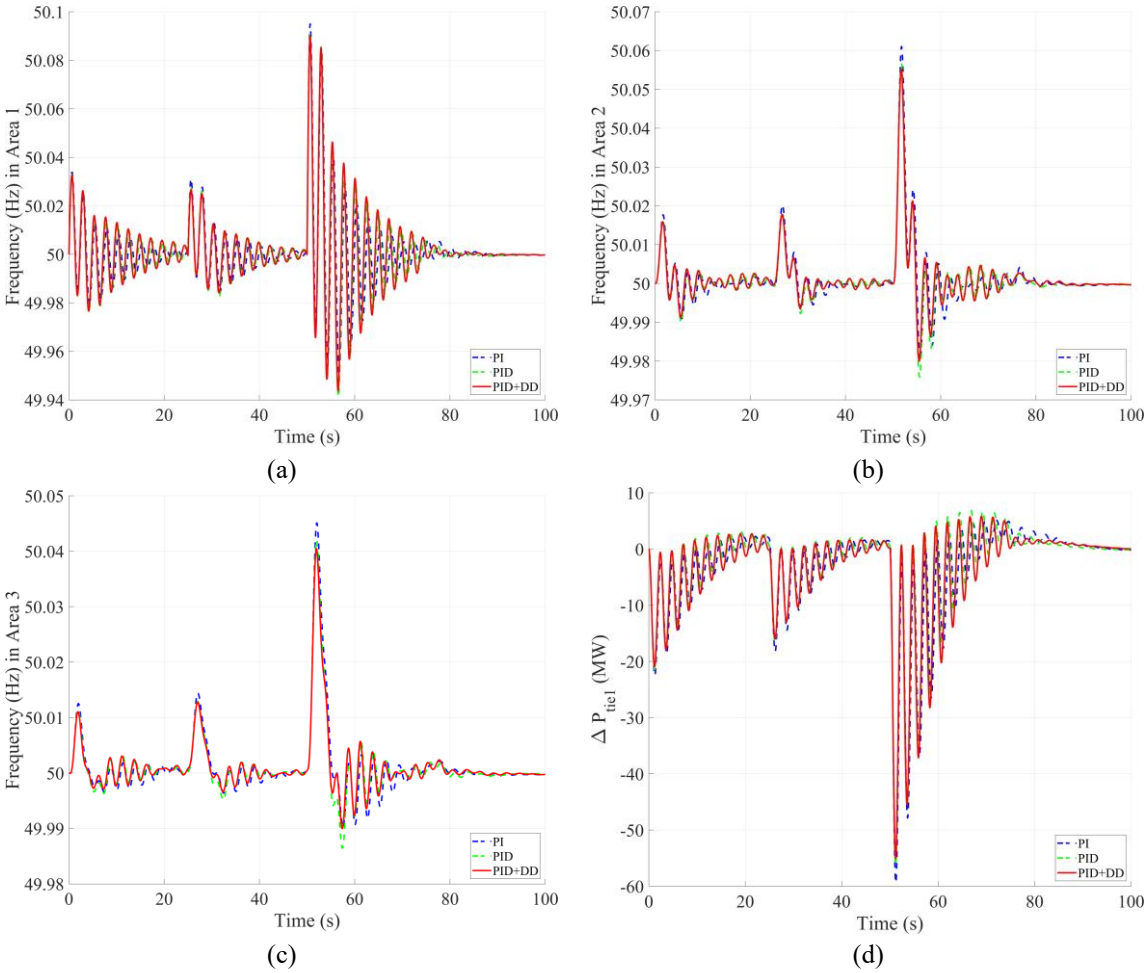

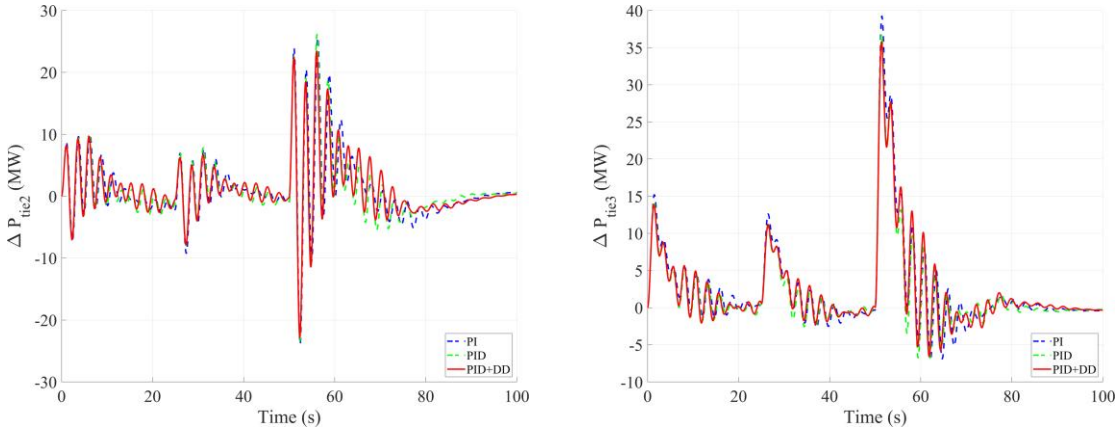

(e) (f)

Fig. 8. Frequency and power deviations in case 2 SLP (a) Frequency deviations in thermal reheat power plants area 1 (b) Frequency deviations in hydropower plants area 2 (c) Frequency deviations in thermal reheat power plants area 3 (d) Power deviations in thermal reheat power plants area 1 (e) Power deviations in hydropower plants area 2 (f) Power deviations in thermal reheat power plants area 3

The Chess Optimizer was used to tune the parameters of controllers such as PI, PID, and PID+DD. In Case Study 1, the optimal values for the PI Controller were Kp1 = 0.1855, Ki1 = 0.1957, Kp2 = 0.3352, Ki2 = 0.7913, Kp3 = 0.9468, and Ki3 = 0.1668. The PID controller parameters are Kp1 = 0.3800, Ki1 = 0.2276, Kd1 = 0.9329, Kp2 = 0.3116, Ki2 = 0.9737, Kd2 = 0.2552, Kp3 = 0.7707, Ki3 = 0.2933, and Kd3 = 0.4850. The PID+DD controller parameters are Kp1 = 0.4138, Ki1 = 0.1759, Kd1 = 0.8804, Kdd1 = 0.6718, Kp2 = 0.3278, Ki2 = 0.9820, Kd2 = 0.0453, Kdd2 = 0.2090, Kp3 = 0.7648, Ki3 = 0.1765, Kd3 = 0.3873, and Kdd3 = 0.4197. The dynamic response in instance 1 is shown in Fig. 8 (a)-(f) and explained in Table 2.

Table 2. The result of case 2

		f_1 (Hz)	f_2 (Hz)	f_3 (Hz)	$P_{tie,1}$ (MW)	$P_{tie,2}$ (MW)	$P_{tie,3}$ (MW)
PID+DD	**Overshoot**	50.0908	50.0563	50.0419	4.5818	25.6945	36.7097
	Undershoot	49.9462	49.9805	49.9884	-55.8819	-22.5097	-5.0278
	Settling time	81.1000	77.8490	78.8000	87.0490	78.8000	63.6467
	ITAE				88.0654		
PID	**Overshoot**	50.0910	50.0566	50.0419	7.1601	25.9306	36.7206
	Undershoot	49.9417	49.9759	49.9865	-56.0374	-23.1340	-7.0392
	Settling time	81.4000	77.5510	78.7510	84.5000	78.3000	64.9000
	ITAE				89.0791		
PI	**Overshoot**	50.0945	50.0609	50.0450	5.2397	25.4599	39.1433
	Undershoot	49.9507	49.9801	49.9902	-59.1707	-23.7012	-7.3825
	Settling time	85.4490	79.7000	78.9510	87.9000	83.3510	67.7268
	ITAE				89.8899		

4. Conclusion

The ITAE analysis indicates that the CO tuned PID+DD controller consistently surpasses both PID and PI controllers across all scenarios. In Case 1 (seen in Fig. 7), PID+DD CO achieved an ITAE of 25.5072, which is 2.7406 lower than PID (9.70% reduction) and 0.5088 lower than PI (1.96% reduction). In Case 2 (seen in Fig. 8), PID+DD CO recorded an ITSE of 88.0654, which is 1.0137 lower than PID (1.14% reduction) and 1.8245 lower than PI (2.03% reduction). In summary, for both cases, the ITAE demonstrated a reduction of approximately 5.42% in comparison to PID and around

1.99% when compared to PI. The results demonstrate that the use of the Chess Optimizer improves oscillation damping and speeds up the dynamic response of systems, especially those facing continuously changing load demands and variable renewable energy generation.

This research examines the implementation of a PID+DD controller in a multi-area power generation system using renewable energy. Adding a second derivative term to the PID controller greatly improves its ability to handle changes in frequency, especially when there are large fluctuations due to the unpredictable nature of renewable energy sources. The PID+DD controller demonstrates superior performance compared to standard controllers (PI and PID) regarding response time, oscillation damping, and overall stability.

The CO was employed to adjust the controller parameters. The experimental findings indicate that CO exhibits superior efficiency in identifying the optimal solution and is more adept at circumventing convergence to local optima compared to established metaheuristic algorithms, highlighting CO's promise in optimizing complex and uncertain control systems.

This research shows how important it is to combine smarter tuning strategies with more flexible controller designs, especially as power systems get more complex. In the future, this approach could be extended to larger networks or adapted to work with other methods like fuzzy logic, predictive control, or even learning algorithms that update in real time-depending on what the grid needs.

Author Contribution: All authors contributed equally to the main contributor to this paper. All authors read and approved the final paper.

Funding: This research project was financially supported by Mahasarakham University, grant number 680012095

Acknowledgment: Thank you to the Faculty of Engineering, Mahasarakham University, for their support and providing facilities, as well as for encouraging study and research.

Conflicts of Interest: The authors declare no conflict of interest.

Appendix

The parameters of the system are f = 50 Hz, n = 100, D_{pi} = 0.01 p.u, D_{fi} = 1 Hz, D_i = 0.01 p.u. MW/Hz, H_i = 5 sec, R_i = p.u. Hz/MW, B_i = 0.4267 p.u. Hz/MW, K_{pi} = 100 Hz/p.u. MW, T_{pi} = 20 sec, T_{ij} = 0.0707 p.u. MW/rad, a_{12} = -1/2, a_{13} = -1/4, a_{23} = -1/2, T_{g1} = 0.08 sec, T_{t1}= 0.4, K_{r1}= 0.33, T_{r1} = 10 sec, T_{h1} = 48.7 sec, T_{h2} = 5, T_{h3} = 0.513 sec, T_w = 1, T_{g3} = 0.08 sec, T_{t3}= 0.4, K_{r3}= 0.33, T_{r3} = 10 sec; Normal Loading 10%. The parameters of wind turbine generation are ρ = 1.225 km/m^3, R_T= 52 m, β = 5 degree, n_r = 10 rpm, $P_{w,max}$ = 10 MW, V_{w1}= 12 m/s, V_{w2}= 15 m/s, C_1= -0.6175, C_2= 116, C_3= 0.4, C_4= 0, C_5= 5, C_6= 21 and C_7= 0.1405.

Author Contribution: All authors contributed equally to the main contributor to this paper. All authors read and approved the final paper.

Funding: This research received no external funding.

Conflicts of Interest: The authors declare no conflict of interest.

References

[1] M. S. Alam *et al*., "High-Level Renewable Energy Integrated System Frequency Control with SMES-Based Optimized Fractional Order Controller," *Electronics*, vol. 10, no. 4, p. 511, 2021, https://doi.org/10.3390/electronics10040511.

[2] Z. Hu, B. Gao, N. Chen, L. Qu, and C. Peng, "Modified virtual synchronous generator based-primary frequency regulation for renewable generation integrated into power system," *IET Generation, Transmission & Distribution*, vol. 14, no. 20, pp. 4435-4443, 2020, https://doi.org/10.1049/iet-gtd.2019.1271.

[3] P. C. Sahu and R. C. Prusty, "Stability Analysis in RECS Integrated Multi-area AGC System with Modified- SOS Optimized Fuzzy Controller," *Recent Advances in Electrical & Electronic Engineering*, vol. 12, no. 6, pp. 532-542, 2019, http://dx.doi.org/10.2174/2352096511666180904113130.

[4] Z. Yan and Y. Xu, "A Multi-Agent Deep Reinforcement Learning Method for Cooperative Load Frequency Control of a Multi-Area Power System," *IEEE Transactions on Power Systems*, vol. 35, no. 6, pp. 4599-4608, 2020, https://doi.org/10.1109/TPWRS.2020.2999890.

[5] Z. He, C. Wan and Y. Song, "Frequency Regulation From Electrified Railway," *IEEE Transactions on Power Systems*, vol. 37, no. 3, pp. 2414-2431, 2022, https://doi.org/10.1109/TPWRS.2021.3119706.

[6] T. Anderson *et al*., "Frequency Regulation With Heterogeneous Energy Resources: A Realization Using Distributed Control," *IEEE Transactions on Smart Grid*, vol. 12, no. 5, pp. 4126-4136, 2021, https://doi.org/10.1109/TSG.2021.3071778.

[7] H. Deeb, A. Sarangi, D. Mishra, and S. Sarangi, "Improved Black Hole optimization algorithm for data clustering," *Journal of King Saud University - Computer and Information Sciences*, vol. 34, no. 8, pp. 5020-5029, 2022, https://doi.org/10.1016/j.jksuci.2020.12.013.

[8] X. Gong *et al*., "Sustainable development of high-performance separation membranes based on green-solvent-processed 2D nanoarchitectured nanofiber/networks," *Chemical Engineering Journal*, vol. 514, p. 163367, 2025, https://doi.org/10.1016/j.cej.2025.163367.

[9] M. Yu *et al*., "Experimental and validation study on the performance and hydrodynamic modelling of a heave attitude self-sustaining wave energy converter," *Energy*, vol. 328, p. 136520, 2025, https://doi.org/10.1016/j.energy.2025.136520.

[10] L. A. C. Minho and W. N. L. dos Santo, "Heterogeneous ensemble learning applied to UV-VIS identification of multi-class pesticides by high-performance liquid chromatography with diode array detector (HPLC/DAD)," *Chemometrics and Intelligent Laboratory Systems*, vol. 261, p. 105385, 2025, https://doi.org/10.1016/j.chemolab.2025.105385.

[11] P. A. Gbadega, Y. Sun, and O. A. Balogun, "Enhanced multi-area automatic generation control in renewable energy-based microgrids using an IPFC-SMES system and COA-optimized FOPID controller," *Energy Reports*, vol. 13, pp. 6479-6513, 2025, https://doi.org/10.1016/j.egyr.2025.05.067.

[12] M. S. Tolba, M. M. Gulzar, A. Arishi, M. Soliman, and A. F. Murtaza, "A novel MPC-based cascaded control for multi-area smart grids: Tackling renewable energy and EV integration challenges," *ISA Transactions*, vol. 165, pp. 143-169, 2025, https://doi.org/10.1016/j.isatra.2025.06.024.

[13] O. Elbaksawi, R. Fathy, A. A. Daoud, and R. A. A. El-aal, "Optimized load frequency controller for microgrid with renewables and EVs based recent multi-objective mantis search algorithm," *Results in Engineering*, vol. 26, p. 105472, 2025, https://doi.org/10.1016/j.rineng.2025.105472.

[14] P. A. Gbadega and Y. Sun, "Multi-area load frequency regulation of a stochastic renewable energy-based power system with SMES using enhanced-WOA-tuned PID controller," *Heliyon*, vol. 9, no. 9, p. e19199, 2023, https://doi.org/10.1016/j.heliyon.2023.e19199.

[15] M. Jalilian, A. Rastgou, S. Kharrati, and S. Hosseini-Hemati, "Load frequency control resilience of hybrid power system with renewable energy sources and superconducting magnetic energy storage using FO-Fuzzy-PID controller," *Results in Engineering*, vol. 27, p. 105961, 2025, https://doi.org/10.1016/j.rineng.2025.105961.

[16] Y. Zheng, J. Tao, Q. Sun, H. Sun, Z. Chen, and M. Sun, "Deep reinforcement learning based active disturbance rejection load frequency control of multi-area interconnected power systems with renewable energy," *Journal of the Franklin Institute*, vol. 360, no. 17, pp. 13908-13931, 2023, https://doi.org/10.1016/j.jfranklin.2022.10.007.

[17] D. Upadhaya, S. Biswas, S. Dutta, and A. Bhattacharya, "Optimal power flow and grid frequency control of conventional and renewable energy source using evolutionary algorithm based FOPID controller," *Renewable Energy Focus*, vol. 53, p. 100676, 2025, https://doi.org/10.1016/j.ref.2024.100676.

[18] A. Sharma and N. Singh, "Load frequency control of connected multi-area multi-source power systems using energy storage and lyrebird optimization algorithm tuned PID controller," *Journal of Energy Storage*, vol. 100, p. 113609, 2024, https://doi.org/10.1016/j.est.2024.113609.

[19] S. Ozumcan, A. Ozturk, M. Varan, and C. Andic, "A novel honey badger algorithm based load frequency controller design of a two-area system with renewable energy sources," *Energy Reports*, vol. 9, pp. 272-279, 2023, https://doi.org/10.1016/j.egyr.2023.10.002.

[20] H. Ahmad, M. M. Gulzar, G. Mustafa, and S. Habib, "AI-based approach for detecting FDI attacks in load frequency control for centralized multi-area power systems," *Computers and Electrical Engineering*, vol. 123, p. 110060, 2025, https://doi.org/10.1016/j.compeleceng.2025.110060.

[21] M. Raju, L. C. Saikia, and N. Sinha, "Automatic generation control of a multi-area system using ant lion Optimizer algorithm based PID plus second order derivative controller," *International Journal of Electrical Power & Energy Systems*, vol. 80, pp. 52-63, 2016, https://doi.org/10.1016/j.ijepes.2016.01.037.

[22] S. Emiroglu and T. E. Gümüş, "Optimal control of automatic voltage regulator system with coronavirus herd immunity Optimizer algorithm-based PID plus second order derivative controller," *Academic Platform Journal of Engineering and Smart Systems*, vol. 10, no. 3, pp. 174-183, 2022, https://doi.org/10.21541/apjess.1149455.

[23] N. Basil *et al*., "Performance analysis of hybrid optimization approach for UAV path planning control using FOPID-TID controller and HAOAROA algorithm," *Scientific Reports*, vol. 15, no. 1, p. 4840, 2025, https://doi.org/10.1038/s41598-025-86803-4.

[24] M. Č. Bošković, T. B. Šekara, and M. R. Rapaić, "Novel tuning rules for PIDC and PID load frequency controllers considering robustness and sensitivity to measurement noise," *International Journal of Electrical Power & Energy Systems*, vol. 114, p. 105416, 2020, https://doi.org/10.1016/j.ijepes.2019.105416.

[25] K. Ullah, A. Basit, Z. Ullah, S. Aslam, and H. Herodotou, "Automatic generation control strategies in conventional and modern power systems: A comprehensive overview," *Energies*, vol. 14, no. 9, p. 2376, 2021, https://doi.org/10.3390/en14092376.

[26] A. D. Sinaiko *et al*., "Out-of-Pocket Spending for Asthma-Related Care Among Commercially Insured Patients, 2004-2016," *The Journal of Allergy and Clinical Immunology: In Practice*, vol. 9, no. 12, pp. 4324-4331.e7, 2021, https://doi.org/10.1016/j.jaip.2021.07.054.

[27] R. Wang, H. Xu, D. Yi, C. Song, and Y. Che, "Automatic detection of Alzheimer's disease from EEG signals using hybrid PSO-GWO algorithm," *Biomedical Signal Processing and Control*, vol. 107, p. 107798, 2025, https://doi.org/10.1016/j.bspc.2025.107798.

[28] J. Águila-León, C. Vargas-Salgado, D. Díaz-Bello, and C. Montagud-Montalvá, "Optimizing photovoltaic systems: A meta-optimization approach with GWO-Enhanced PSO algorithm for improving MPPT controllers," *Renewable Energy*, vol. 230, p. 120892, 2024, https://doi.org/10.1016/j.renene.2024.120892.

[29] N. Elghardouf, Y. Ennaciri, A. Elakkary, and N. Sefiani, "Multi-loop active disturbance rejection control and PID control strategy for poultry house based on GA, PSO and GWO algorithms," *Heliyon*, vol. 10, no. 8, p. e29579, 2024, https://doi.org/10.1016/j.heliyon.2024.e29579.

[30] J. Wang, Q.-Y. Guo, C.-L. Fu, G. Dai, C.-Y. Xia, and L.-Q. Qian, "A novel optimization scheme for structure and balance of compound balanced beam pumping units using the PSO, GA, and GWO algorithms," *Petroleum Science*, vol. 22, no. 3, pp. 1340-1359, 2025, https://doi.org/10.1016/j.petsci.2025.01.007.

[31] S. Audomsi, S. Wattana, N. Uthathip, and W. Sa-ngiamvibool, "Development and Design of an Optimal Fuzzy Logic Two Degrees of Freedom-Proportional Integral Derivative Controller for a Two-Area Power System Using the Bee Algorithm," *Energies*, vol. 18, no. 4, p. 915, 2025, https://doi.org/10.3390/en18040915.

[32] Y. He and N. Xian, "Short-term optimal scheduling of hydro–wind–PV and multi-storage complementary systems based on opposition-based learning PSO algorithm," *Applied Energy*, vol. 394, p. 126125, 2025, https://doi.org/10.1016/j.apenergy.2025.126125.

[33] S. V. Thambi, I. G, K. S. Kammari, and A. Sahay, "Hybrid Metaheuristic Optimisation for Lung Cancer Image Classification: Leveraging MOEA, PSO, and ACO Algorithms," *Procedia Computer Science*, vol. 258, pp. 3781-3793, 2025, https://doi.org/10.1016/j.procs.2025.04.633.

[34] Z. Liu *et al*., "Enhancing XRF sensor-based sorting of porphyritic copper ore using particle swarm optimization-support vector machine (PSO-SVM) algorithm," *International Journal of Mining Science and Technology*, vol. 34, no. 4, pp. 545-556, 2024, https://doi.org/10.1016/j.ijmst.2024.04.002.

[35] K. P. Sanoj and V. Dhanya Ram, "Optimal PID Controller Tuning for Multivariable Unstable Systems by Minimizing ITAE Criteria," *IFAC-PapersOnLine*, vol. 57, pp. 391-396, 2024, https://doi.org/10.1016/j.ifacol.2024.05.067.

[36] C. S. Rao, S. Santosh, and D. R. V, "Tuning optimal PID controllers for open loop unstable first order plus time delay systems by minimizing ITAE criterion," *IFAC-PapersOnLine*, vol. 53, no. 1, pp. 123-128, 2020, https://doi.org/10.1016/j.ifacol.2020.06.021.

[37] Y. Nie, Y. Zhang, Y. Zhao, B. Fang, and L. Zhang, "Wide-area optimal damping control for power systems based on the ITAE criterion," *International Journal of Electrical Power & Energy Systems*, vol. 106, pp. 192-200, 2019, https://doi.org/10.1016/j.ijepes.2018.09.036.

[38] V. P. Meena, V. P. Singh, and J. M. Guerrero, "Investigation of reciprocal rank method for automatic generation control in two-area interconnected power system," *Mathematics and Computers in Simulation*, vol. 225, pp. 760-778, 2024, https://doi.org/10.1016/j.matcom.2024.06.007.

[39] R. R. Shukla, M. M. Garg, A. K. Panda, and D. Das, "Enhancing load frequency control with plug-in electric vehicle integration in non-reheat thermal power systems," *Electrical Engineering*, vol. 106, no. 3, pp. 3305-3320, 2024, https://doi.org/10.1007/s00202-023-02144-3.

[40] R. Kumar and A. Sikander, "A novel load frequency control of multi area non-reheated thermal power plant using fuzzy PID cascade controller," *Sādhanā*, vol. 48, no. 1, p. 25, 2023, https://doi.org/10.1007/s12046-022-02071-2.

[41] B. Sun *et al*., "Thermodynamic performance analysis of steam power plants during deep peak shaving processes: Integrating a novel top turbine system in ultra-low loads," *Energy*, vol. 315, p. 134425, 2025, https://doi.org/10.1016/j.energy.2025.134425.

[42] W. Ji *et al*., "A real-time phase transition modeling of supercritical steam cycle and load variation rate enhancement of thermal power plants under deep peak shaving," *Energy*, vol. 312, p. 133431, 2024, https://doi.org/10.1016/j.energy.2024.133431.

[43] R. Irfan *et al*., "Robust operating strategy for voltage and frequency control in a non-linear hybrid renewable energy-based power system using communication time delay," *Computers and Electrical Engineering*, vol. 123, p. 110119, 2025, https://doi.org/10.1016/j.compeleceng.2025.110119.

[44] D. Mokeddem and S. Mirjalili, "Improved Whale Optimization Algorithm applied to design PID plus second-order derivative controller for automatic voltage regulator system," *Journal of the Chinese Institute of Engineers*, vol. 43, no. 6, pp. 541-552, 2020, https://doi.org/10.1080/02533839.2020.1771205.

[45] S. Lalngaihawma, S. Datta, S. Das, F. Alsaif and T. S. Ustun, "Automatic Generation Control of Hybrid Sources Incorporating Renewable Energy Sources and Electric Vehicles in an Interconnected Power System Considering a Deregulated Environment," *IEEE Access*, vol. 12, pp. 124764-124789, 2024, https://doi.org/10.1109/ACCESS.2024.3454229.

[46] A. N. Karanam and B. Shaw, "A new two-degree of freedom combined PID controller for automatic generation control of a wind integrated interconnected power system," *Protection and Control of Modern Power Systems*, vol. 7, no. 2, pp. 1-16, 2022, https://doi.org/10.1186/s41601-022-00241-2.

[47] G. Li, J. Zhang, X. Wu and X. Yu, "Small-Signal Stability and Dynamic Behaviors of a Hydropower Plant With an Upstream Surge Tank Using Different PID Parameters," *IEEE Access*, vol. 9, pp. 104837-104845, 2021, https://doi.org/10.1109/ACCESS.2021.3097500.

[48] V. Häberle, M. W. Fisher, E. Prieto-Araujo and F. Dörfler, "Control Design of Dynamic Virtual Power Plants: An Adaptive Divide-and-Conquer Approach," *IEEE Transactions on Power Systems*, vol. 37, no. 5, pp. 4040-4053, 2022, https://doi.org/10.1109/TPWRS.2021.3139775.

[49] M. M. Gulzar, M. Iqbal, S. Shahzad, H. A. Muqeet, M. Shahzad, and M. M. Hussain, "Load frequency control (LFC) strategies in renewable energy-based hybrid power systems: A review," *Energies*, vol. 15, no. 10, p. 3488, 2022, https://doi.org/10.3390/en15103488.

[50] J. I. Sarasua, G. Martínez-Lucas, H. García-Pereira, G. Navarro-Soriano, Á. Molina-García, and A. Fernández-Guillamón, "Hybrid frequency control strategies based on hydro-power, wind, and energy storage systems: Application to 100% renewable scenarios," *IET Renewable Power Generation*, vol. 16, no. 6, pp. 1107-1120, 2022, https://doi.org/10.1049/rpg2.12326.

[51] X. Wang, Y. Wang, and Y. Liu, "Dynamic load frequency control for high-penetration wind power considering wind turbine fatigue load," *International Journal of Electrical Power & Energy Systems*, vol. 117, p. 105696, 2020, https://doi.org/10.1016/j.ijepes.2019.105696.

[52] C. Wu, X. -P. Zhang and M. Sterling, "Wind power generation variations and aggregations," *CSEE Journal of Power and Energy Systems*, vol. 8, no. 1, pp. 17-38, 2022, https://doi.org/10.17775/CSEEJPES.2021.03070.

[53] M. A. Hossain, R. K. Chakrabortty, S. Elsawah, and M. J. Ryan, "Very short-term forecasting of wind power generation using hybrid deep learning model," *Journal of Cleaner Production*, vol. 296, p. 126564, 2021, https://doi.org/10.1016/j.jclepro.2021.126564.

[54] S. Tanarat *et al*., "Enhancing Small and Medium Enterprises in Phayao, Thailand: Socio-Economic Impact of Greenhouse Solar Drying for Andrographis Paniculata," *Engineering Access*, vol. 11, no. 1, pp. 141-150, 2025, https://ph02.tci-thaijo.org/index.php/mijet/article/view/254533.

[55] M. M. Sulaiman, Z. Al-Khafaji, Z. N. Shareef, and M. Falah, "Carbon Capture Based on Chemical Absorption: Process Design and Techno-Economic Assessments," *Engineering Access*, vol. 11, no. 1, pp. 57-64, 2025, https://ph02.tci-thaijo.org/index.php/mijet/article/view/253944.

[56] P. Kailomsom, P. Nasawat, W. Khunthirat, and W. Phuangpornpitak, "A Hybrid Method based on BWM and TOPSIS-LP Model to Assess Computer Numerical Control Machines," *Engineering Access*, vol. 11, no. 1, pp. 108-118, 2025, https://ph02.tci-thaijo.org/index.php/mijet/article/view/254158.

[57] Y. Gui, H. Song, J. Yang, and C. Qiu, "Data-driven discovery of the design rules for considering the curing deformation and the application on double-double composites," *Composites Part C: Open Access*, vol. 17, p. 100612, 2025, https://doi.org/10.1016/j.jcomc.2025.100612.

[58] S. A. Alnefaie, A. Alkuhayli, and A. M. Al-Shaalan, "Optimizing Load Frequency Control of Multi-Area Power Renewable and Thermal Systems Using Advanced Proportional–Integral–Derivative Controllers and Catch Fish Algorithm," *Fractal and Fractional*, vol. 9, no. 6, p. 355, 2025, https://doi.org/10.3390/fractalfract9060355.

[59] M. Tomasik, S. Lis, and A. Tarniowy, "Optimization of the bioethanol production process control algorithm in terms of designing the guideline executive systems," *Przemysl Chemiczny*, vol. 104, no. 5, pp. 545-548, 2025, https://doi.org/10.15199/62.2025.5.1.

[60] T. Kinoshita and T. Yamamoto, "Design of a Database-Driven PID Controller using the Estimated Input/Output Data," *IFAC-PapersOnLine*, vol. 58, no. 14, pp. 700-705, 2024, https://doi.org/10.1016/j.ifacol.2024.08.419.

[61] M. Micev, M. Ćalasan and M. Radulović, "Optimal design of real PID plus second-order derivative controller for AVR system," *2021 25th International Conference on Information Technology (IT)*, pp. 1-4, 2021, https://doi.org/10.1109/IT51528.2021.9390145.

[62] B. V. S. Acharyulu and V. S. S. A. K. Nayani, "Sea Lion Optimized PID + DD Controller for Load Frequency Control of a Hybrid Power System," *SN Computer Science*, vol. 4, no. 5, p. 567, 2023, https://doi.org/10.1007/s42979-023-02009-3.